Characterization of Vinyl Polymer/Silica Colloidal Nanocomposites Using Solid State NMR Spectroscopy: Probing the Interaction between the Inorganic and Organic Phases on the Molecular Level

Gyan K. Agarwal and Jeremy J. Titman*

School of Chemistry, University of Nottingham, University Park, Nottingham NG7 2RD, U.K.

Matthew J. Percy and Steven P. Armes*

Department of Chemistry, School of Life Sciences, University of Sussex, Falmer, Brighton BN1 9QJ, U.K.

Received: July 16, 2003; In Final Form: September 5, 2003

Colloidal poly(4-vinylpyridine)/silica and polystyrene/silica nanocomposite particles comprising 38% and 48% silica by mass, respectively, have been characterized by solid-state NMR spectroscopy in order to probe the nature of the molecular interactions between the polymer and silica phases. For P4VP/silica nanocomposite particles, our results indicate hydrogen bond formation between the pyridine nitrogen and a surface hydroxyl proton. In contrast, a π-interaction between the aromatic ring and the silica surface is the most likely model for the PS/silica nanocomposite particles. Nonspecific binding interactions do not appear to play an important role in nanocomposite particle formation in either case. The high-resolution proton−carbon-13 and proton−silicon-29 correlation experiments used to extract this information are a novel combination of multipulse proton decoupling and Lee−Goldberg cross-polarization.

Introduction

Organic/inorganic hybrids offer the possibility of a new generation of nanostructured materials with diverse applications such as catalysts,[1] electronic or photonic devices,[2] and sensors for volatile organic compounds.[3] Furthermore, the incorporation of inorganic materials on the nanoscale can enhance the fire retardancy[4] and mechanical strength[5] of organic polymers and coatings. In recent years there has been increasing interest in the synthesis of *particulate* or *colloidal* organic/inorganic hybrids.[6] For example, Armes and co-workers have developed the "surfactant-free" synthesis of vinyl polymer/silica nanocomposite particles by (co)polymerizing 4-vinylpyridine (4VP) in the presence of an ultrafine aqueous silica sol.[7−10] A minimum proportion of 4VP comonomer is essential to ensure a sufficiently strong interaction between the organic and inorganic phases, but most of the 4VP can be replaced with styrene, methyl methacrylate, or *n*-butyl acrylate to produce more cost-effective formulations which can be either film-forming or non-film-forming according to the copolymer composition. More recently, Percy and Armes have shown that the use of an alcoholic silica sol allows colloidally stable nanocomposite particles to be prepared in the *absence* of the 4-vinylpyridine auxiliary.[11] This new approach is now being exploited to prepare poly(methyl methacrylate)/silica and polystyrene/silica nanocomposites. Typically, these hybrid particles range from 100 to 200 nm diameter and, depending on the formulation, contain approximately 10−50% silica by mass.

In the present work solid-state NMR spectroscopy was used to investigate the molecular interaction between the polymer and silica phases for these two classes of vinyl polymer/silica colloidal nanocomposites. The representative samples chosen were poly(4-vinylpyridine) (P4VP)/silica particles prepared using an aqueous silica sol and polystyrene (PS)/silica particles prepared using an alcoholic silica sol (Figure 1). Samples with the opposite polymer−silica sol pairings which would allow a more complete investigation cannot be synthesized, and the relative merits and applicability of the aqueous and alcoholic silica sols have been discussed previously.[11] A possible adsorption mode for P4VP/silica is a lone pair interaction between the pyridine nitrogen atom and the hydroxyl protons on the silica surface. An alternative would be a π-interaction involving the pyridine ring. Likely interactions for PS/silica include a π-interaction involving the benzene ring or a less specific van der Waals interaction between the aliphatic polymer chain backbone and the silica surface. Two of these possibilities are illustrated schematically in Figure 2. High-resolution proton−carbon-13 and proton−silicon-29 correlation experiments were used in combination to assign the proton resonances in the nanocomposites, using the original silica sols and the P4VP and

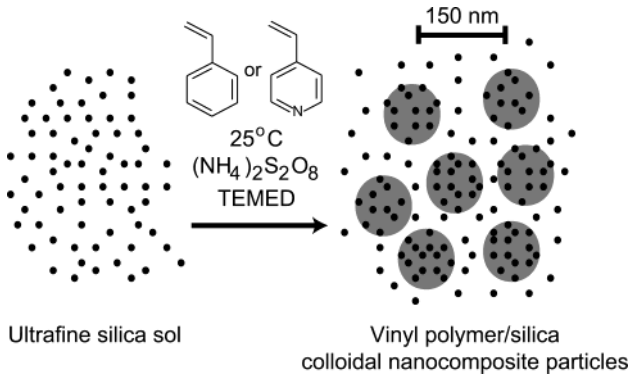

Figure 1. Schematic representation of the synthesis of the colloidal nanocomposite particles by the in situ homopolymerization of either 4-vinylpyridine or styrene in the presence of an aqueous 20 nm silica sol (4-vinylpyridine) or an alcoholic 13 nm silica sol (styrene).

* To whom correspondence should be addressed.

10.1021/jp036065g CCC: $25.00
Published on Web 10/17/2003

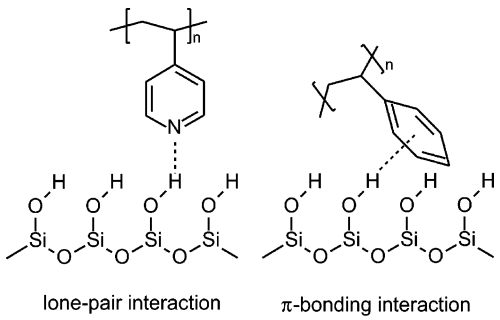

Figure 2. Possible modes of interaction between the polymer and silica phases in the two nanocomposites investigated in this study.

PS homopolymers as reference materials. Since these experiments were designed so that proton polarization is transferred selectively to near-neighbor heteronuclei only, the proton−silicon-29 variant was also used to assess the proximity of protons to the silica surface. This information, together with the proton assignment, allowed conclusions to be drawn about the nature of the polymer−silica interaction.

Experimental Section

Reagents. Nyacol 2040 (a 20 nm aqueous silica sol, supplied as a 40 w/v % solution by Eka Chemicals, Bohus, Sweden) and IPA-ST (a 13 nm silica sol dispersed in 2-propanol, supplied as a 30 w/v % solution by Nissan Chemicals, USA) were used as received. Styrene (Aldrich) and 4-vinylpyridine (Aldrich) were distilled under reduced pressure; both purified monomers were stored at −20 °C prior to use.

Nanocomposite Syntheses. The P4VP/silica nanocomposite was prepared by the free radical homopolymerization of 4-vinylpyridine in the presence of the 20 m aqueous silica sol under emulsion polymerization conditions. 4-Vinylpyridine (5.0 mL), Nyacol 2040 silica sol (19.0 g aqueous solution, equivalent to 8.0 g of dry silica), and water (73 mL) were added to a three-necked round-bottomed flask. This reaction mixture was purged with nitrogen and heated to 60 °C. An aqueous solution of ammonium persulfate initiator (1.0 wt % based on monomer) was added to the reaction vessel, and the mixture was stirred mechanically for 24 h under a nitrogen atmosphere.

The PS/silica nanocomposite was prepared as follows. IPA-ST silica sol (13.3 g of IPA solution, equivalent to 4.0 g of dry weight silica) was mixed with deionized water (31.0 mL) and styrene (2.5 mL) in a Schott bottle that contained a magnetic flea. The jar was sealed with a rubber septum to allow both degassing and also addition of the initiator via syringe needles. The mixture was degassed with nitrogen and placed in a circulating water bath maintained at 25 °C equipped with a magnetic stirrer. Ammonium persulfate initiator (APS) (25.0 mg, 1.0 wt % based on monomer) dissolved in water (1.5 mL) and *N*,*N*,*N*′,*N*′-tetramethylethylenediamine (TEMED, the APS/TEMED molar ratio was unity) dissolved in water (1.5 mL) were separately degassed and added to the reaction vessel. The reaction mixture was stirred at 25 °C for 24 h.

Purification of both the above nanocomposite dispersions was achieved by repeated centrifugation−redispersion cycles, with the supernatants being discarded. P4VP/silica nanocomposites were redispersed in mildly alkaline aqueous solution (pH 10), and PS/silica nanocomposites were redispersed in mildly acidic solution (pH 4). Care was taken to avoid excessive centrifugation rates and times that would otherwise result in the unwanted sedimentation of the excess silica sol and also make redispersion of the nanocomposite particles more difficult. This centrifugation−redispersion protocol was continued (at least three cycles) until TEM examination confirmed the absence of excess silica sol.

Nanocomposite Characterization. *Particle Size Analysis.* Disk centrifuge photosedimentometry (DCP; Brookhaven Instruments) was used to obtain the weight-average particle size distributions of the nanocomposite particles. Solid-state particle densities were measured by helium pycnometry (Micromeritics AccuPyc 1330 instrument). The centrifugation rate was in the 3000−12000 rpm range, and the dispersions were assumed to have the same scattering characteristics as aqueous polystyrene latex. Typical DCP runs lasted 30 min. Dynamic light scattering (DLS) measurements were performed on a Malvern 4700 instrument equipped with a 75 mW argon ion laser; all measurements were carried out at 25 °C at a fixed angle of 90° on highly dilute aqueous solutions.

Surface Area Analysis and Density Measurements. BET surface area measurements were performed on a Quantachrome Nova 1000 instrument using dinitrogen as an adsorbate at 77 K. The area per molecule for dinitrogen was taken to be 16.2 Å^2. This protocol gave a specific surface area of 163 m^2 g^{-1} for the Nyacol 2040 silica sol and 220 m^2 g^{-1} for the Nissan IPA-ST silica sol. Helium pycnometry (Micromeritics AccuPyc 1330 instrument) measurements indicated densities of 2.17 and 2.13 g cm^{-3} for the dried Nyacol 2040 and Nissan IPA-ST silica sols, respectively. Using $A_s = 6/\rho D$, where A_s is the BET specific surface area, ρ is the particle density, and D is the particle diameter, mean particle diameters of 17 nm for the Nyacol 2040 sol and 13 nm for the Nissan IPA-ST sol were calculated. These values are in reasonably good agreement with the nominal diameters of 20 nm (Nyacol 2040 sol) and 13 nm (Nissan IPA-ST sol) provided by the manufacturers.

Scanning Electron Microscopy. Nanocomposite particles were deposited onto specimen stubs and sputter-coated with gold prior to examination using a Leica Stereoscan 420 instrument.

Chemical Composition. Thermogravimetric analyses were performed using a Perkin-Elmer TGA-7 instrument. Nanocomposite dispersions were dried at 50 °C overnight to yield dried powders. These powders were heated in air to 800 °C at a scan rate of 20 °C min^{-1}, and the observed mass loss was attributed to the quantitative pyrolysis of the (co)polymer component. The incombustible residues remaining after pyrolysis were assumed to be pure silica (SiO_2), and the inorganic contents of the nanocomposites were calculated after correcting for loss of surface moisture of the silica sol at elevated temperature. CHN microanalyses were carried out at an independent external analytical laboratory (Medac Ltd., Egham, Surrey, U.K.).

Solid-State NMR Spectroscopy. The pulse sequence that was used to record the high-resolution heteronuclear correlation spectra is shown in Figure 3. At the start of the preparation period carbon-13 or silicon-29 spins are saturated by a small number of 90° pulses separated by delays that are short compared to the spin−lattice relaxation time. Subsequently, a 90° pulse generates proton transverse magnetization that evolves during t_1 under the windowless BLEW-12 homonuclear decoupling sequence.[12] Simultaneously, the windowless BB-24 sequence[13] is applied to carbon-13 or silicon-29 with the Hartmann−Hahn condition fulfilled, such that its twenty-four 90° pulses are in synchrony with the twenty-four proton 90° pulses which comprise two cycles of BLEW-12. The combined effect of simultaneous application of BLEW-12 and BB-24 is to suppress both heteronuclear and homonuclear dipolar interactions, resulting in a well-resolved proton spectrum in ω_1. To avoid interference between the decoupling sequences and MAS,

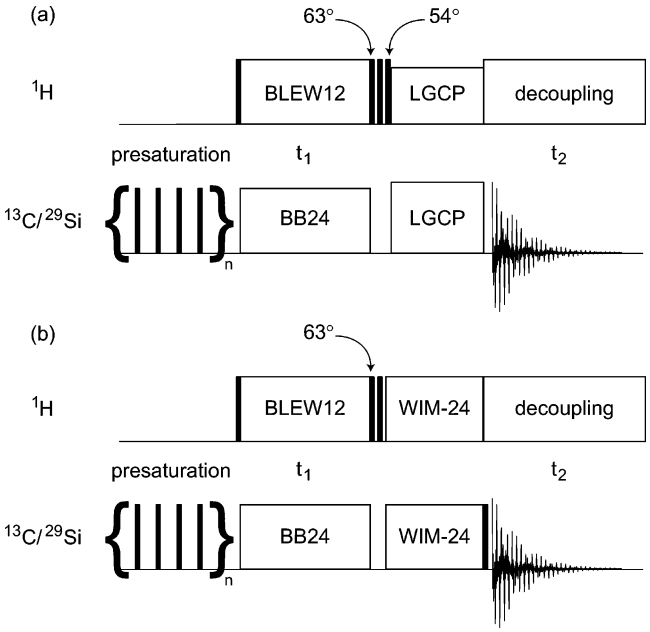

Figure 3. Pulse sequences used to record high-resolution proton−carbon-13 and proton−silicon-29 correlation spectra in this work. Polarization transfer is achieved in part a by Lee−Goldberg cross-polarization and in part b by a WIM-24 multipulse sequence. Filled bars represent 90° pulses unless otherwise indicated.

the rf field strength is chosen such that the MAS period is an integer multiple of the BB-24 cycle time. Since the effective magnetic field for BLEW-12 is tilted at 63° from the *z*-axis, the proton chemical shift in ω_1 is scaled by a factor of 0.475.

The mixing period is initiated by two proton pulses in quadrature with flip angles of 63° and 90°, respectively, which rotate one component of the proton magnetization precessing about the tilted field under BLEW-12 onto the *z*-axis. Transfer of this component to neighboring heteronuclear spins is achieved using either Lee−Goldberg cross-polarization (LG-CP)[14] or the WIM-24 isotropic mixing sequence.[15] Both of these methods result in selective magnetization transfer from nearby protons by suppressing spin diffusion. For LG-CP (Figure 3a) the proton magnetization is rotated by an additional pulse of flip angle 54.7°, before spin locking in an effective magnetic field tilted at the same angle from the *z*-axis. During the spin-lock pulse a carbon-13 or silicon-29 rf field is applied at the Hartmann−Hahn condition to effect magnetization transfer. For WIM-24 (Figure 3b) the two initial mixing pulses are sufficient, since the isotropic nature of the sequence ensures longitudinal proton magnetization is transferred to carbon-13 or silicon-29. In this case an additional 90° pulse on the heteronucleus after the WIM-24 sequence produces observable magnetization. The carbon-13 or silicon-29 FID is detected as usual with proton decoupling during t_2. The TPPI method is used to obtain pure absorption two-dimensional line shapes, and the phases of all the proton pulses up to and including the first pulse of the mixing period are incremented by 90°.

It should be noted that more straightforward methods for obtaining high-resolution heteronuclear correlation spectra based on rapid MAS are not appropriate for the materials studied here, since large sample volumes and therefore slow spinning rates are required to obtain sufficient sensitivity.

High-resolution proton−carbon-13 and proton−silicon-29 correlation spectra were recorded for P4VP/silica and PS/silica nanocomposites at a Larmor frequency of 300.07 MHz for protons, using a standard double-resonance MAS probe with 7.5 mm external diameter rotors. No attempt was made to restrict the samples within the rotor to avoid the adverse effects of B_1 inhomogeneity. The proton pulse lengths were carefully calibrated prior to each experiment using a restricted sample of silicone rubber, and asymmetric phase transients were eliminated by slightly detuning the probe and proton amplifier according to standard procedures.[16] Proton pulse lengths of typically 3.7 μs were used for the BLEW-12 sequence. The carbon-13 and silicon-29 rf field strengths required for the simultaneous BB-24 sequence were found from the corresponding Hartmann−Hahn condition for the nanocomposite sample. The t_1 dwell time was typically 88.8 μs, resulting in a ω_1 spectral width of 5.63 kHz that corresponds to a total range of 39.5 ppm for protons when the BLEW-12 scaling factor is taken into account. The proton rf offset during the BLEW-12 sequence was the same in all experiments. The MAS rate was set so that the spinning was synchronized with the BLEW-12 sequence as described above, typically either 3.75 kHz or 2.81 kHz. For LG-CP the proton frequency offset was 40 kHz with the proton rf field strength reduced to achieve an effective field at 54.7°, and the cross-polarization time was 1 ms for proton−silicon-29 experiments. For WIM-24 the pulse length and rf field strengths were identical to those used for BLEW-12 and BB-24, and a single cycle was used for proton−carbon-13 experiments. The t_2 acquisition time was 20.5 ms with a dwell time of 20 μs. Chemical shifts in the ω_2 dimension were referenced externally to TMS for both carbon-13 and silicon-29, while in the ω_1 dimension the reference was the adamantane proton resonance. There were 256 or 1024 scans for proton−carbon-13 or proton−silcon-29 experiments, respectively, and 32 t_1 increments. A relaxation delay of 4 s was inserted between scans, and presaturation was achieved by a sequence of 10 carbon-13 or silicon-29 90° pulses separated by a 10 ms delay.

Results and Discussion

Table 1 provides a convenient summary of the synthesis details of the two nanocomposites, as well as their mean particle size, silica content, and particle density. The P4VP/silica nanocomposite was synthesized as described previously,[8] whereas the PS/silica nanocomposite was prepared using a similar protocol to that reported for the synthesis of poly(methyl methacrylate)/silica nanocomposite particles.[11] Thermogravimetry analyses indicated silica contents of 38% and 48% by mass for the P4VP/silica and PS/silica nanocomposites, respectively. Particle densities of 1.49 and 1.40 g cm^{-3} were determined using helium pycnometry. At first sight, these densities appear anomalous given the silica contents of the nanocomposites, but the higher density obtained for the P4VP/silica nanocomposite simply reflects the higher density of poly(4-vinylpyridine) (1.20 g cm^{-3}) compared to that of polystyrene (1.05 g cm^{-3}). Dynamic light scattering (DLS) studies of the diluted reaction solutions gave intensity-average particle diameters of 200 and 180 nm for the P4VP/silica and PS/silica nanocomposites, respectively. The similarity between these values and the corresponding weight-average particle diameters of 140 ± 30 nm reported by disk centrifuge photosedimentometry (DCP) indicate high degrees of dispersion (i.e. minimal flocculation) for both colloidal nanocomposites. Electron micrographs of the P4VP/silica nanocomposites have been reported previously.[7,8] A typical scanning electron micrograph depicting the PS/silica nanocomposite particles is shown in Figure 4. The particle size distribution is reasonably uniform, and the mean number-average particle diameter of 140 nm is in reasonably good agreement with the data obtained by DLS and DCP.

Silicon-29 CPMAS spectra of the dried Nyacol silica sol (a) and the P4VP/silica nanocomposite (b) recorded with a cross-

TABLE 1: Summary of the Synthesis Conditions, Particle Densities, Silica Contents, and Particle Diameters of the Two Vinyl Polymer/Silica Nanocomposites Examined in This Study

monomer type	silica type	polymerization medium	initiator system	reaction temp, °C	density,[a] g cm^{-3}	silica content,[b] wt %	particle diameter, nm		
							DLS[c] D_n	DCP[d] D_w	TEM D_n
4VP	Nyacol 2040	water	APS	60	1.49	38	200	140 ± 30	130
styrene	Nissan IPA-ST	74:26 v/v water/IPA	1:1 APS/TEMED	25	1.40	48	180	140 ± 30	140

[a] As measured by helium pycnometry (Micromeritics Accupyc 1330 instrument). [b] By thermogravimetric analysis in air at a scan rate of 20 °C/min, assuming that the incombustible residues are silica (SiO_2). [c] Intensity-average particle diameter determined by dynamic light scattering studies of the diluted reaction solutions. [d] Weight-average particle diameter reported by disk centrifuge photosedimentometry studies of the purified nanocomposite particles after several centrifugation−redispersion cycles to remove the excess silica sol.

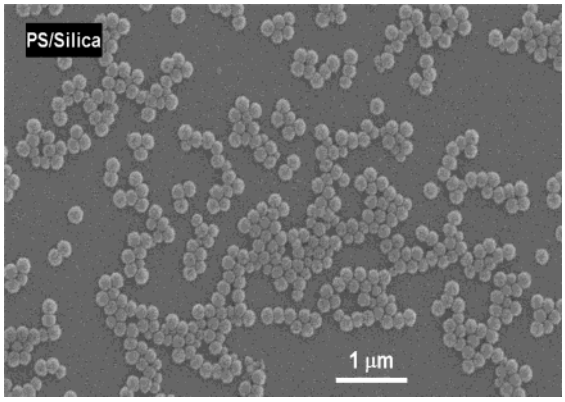

Figure 4. Typical scanning electron micrograph of the PS/silica nanocomposite particles studied in this work.

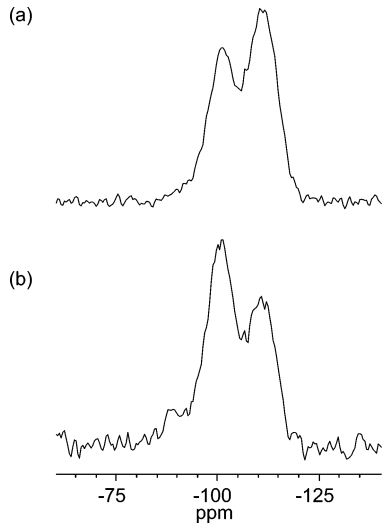

Figure 5. Silicon-29 CPMAS spectra of (a) a dried Nyacol silica sol and (b) the P4VP/silica nanocomposite recorded using the parameters described in the text.

polarization time of 5 ms are shown in Figure 5. These consist of two clearly resolved resonances at approximately $\delta = -100$ and -110 ppm, respectively, with a low intensity unresolved shoulder at $\delta = -90$ ppm. These three peaks appear at similar shifts to those observed for silica gel[17] and can be assigned to surface silicon bound to a single hydroxyl group, bulk silicon, and surface silicon bound to two hydroxyl groups, respectively. The variation in intensity of these three peaks with cross-polarization time confirms this assignment. At a cross-polarization time of 5 ms the bulk silicon resonance at $\delta = -110$ ppm is more intense than the surface silicon resonance at $\delta = -100$ ppm for myacol, while for the nanocomposite the opposite is the case. This suggests that, on average, the protons responsible for cross-polarization in the nanocomposite are further from the silica surface. Hence, at least part of the silicon-29 polarization originates from the polymer protons. Similar silicon-29 CPMAS spectra were obtained for the dehydrated IPA-ST silica sol and the PS/silica nanocomposite.

Figure 6a shows a WIM-24 high-resolution proton−carbon-13 correlation spectrum of the P4VP/silica nanocomposite, recorded with a single mixing cycle of WIM-24 which ensures that correlations are limited to directly bonded proton−carbon-13 pairs. The carbon-13 skyline projection (top) is similar to the carbon-13 CPMAS spectrum observed for poly(4-vinylpyridine). Spinning sidebands are distinguished by an asterisk. The isotropic peak at $\delta = 149$ ppm is assigned to the pyridine carbon adjacent to nitrogen, with the other two ring sites at $\delta = 124$ ppm and the polymer main chain carbons at around $\delta = 40$ ppm. Pyridine ring and aliphatic main chain proton resonances are resolved in the high-resolution proton projection (right) with the latter at $\delta = 1.3$ ppm. However, the extra dispersion gained from the carbon-13 chemical shift in the two-dimensional spectrum allows the two pyridine proton sites to be distinguished, with the protons closest to nitrogen at around $\delta = 8.3$ ppm and the other aromatic protons at $\delta = 6.3$ ppm. These values agree fairly well with the proton chemical shifts for pyridine in solution. Figure 6b shows a LG-CP high-resolution proton−silicon-29 correlation spectrum of the dried Nyacol silica sol starting material. The silicon-29 ω_2 skyline projection (top) shows the three peaks observed in the silicon-29 CPMAS spectrum in Figure 5. It should be noted that with 1 ms of Lee−Goldberg cross-polarization the surface silica peak is now the most intense and that additional line broadening was used here to give an acceptable signal-to-noise ratio. The two-dimensional spectrum shows that both surface and bulk silicon-29 resonances correlate with a broad proton line at around $\delta = 5.5$ ppm in the ω_1 skyline projection (right). Hence, this δ value corresponds to hydroxyl protons on the silica surface.

Figure 6c shows a LG-CP high-resolution proton−silicon-29 correlation spectrum of the P4VP/silica nanocomposite. In the silicon-29 ω_2 skyline projection the surface silicon site dominates, while in the proton ω_1 skyline projection three resonances are visible at around $\delta = 6$, 8.5, and 11 ppm, respectively. It should be noted that there are no correlations between silicon-29 nuclei and protons in the aliphatic part of the spectrum, below $\delta = 5$ ppm. Hence, a possible nonspecific van der Waals interaction with parts of the polymer main chain in close proximity with the silica surface can be ruled out. Of the three proton lines, that at $\delta = 6$ ppm is predominantly responsible for cross-polarizing the bulk silicon-29 nuclei. Since a similar $\delta = 5.5$ ppm proton shift is also observed for the pristine Nyacol silica sol, this $\delta = 6$ ppm signal is assigned to surface hydroxyl protons. All three proton resonances correlate with the surface silicon site. Using the polymer proton shifts obtained from the high-resolution proton−carbon-13 correlation spectrum shown in Figure 6a, the most intense of the three lines at $\delta = 8.5$ ppm can be assigned to the pyridine protons adjacent to nitrogen. This implies that there is a specific interaction between the silica surface and the nitrogen lone pair of the

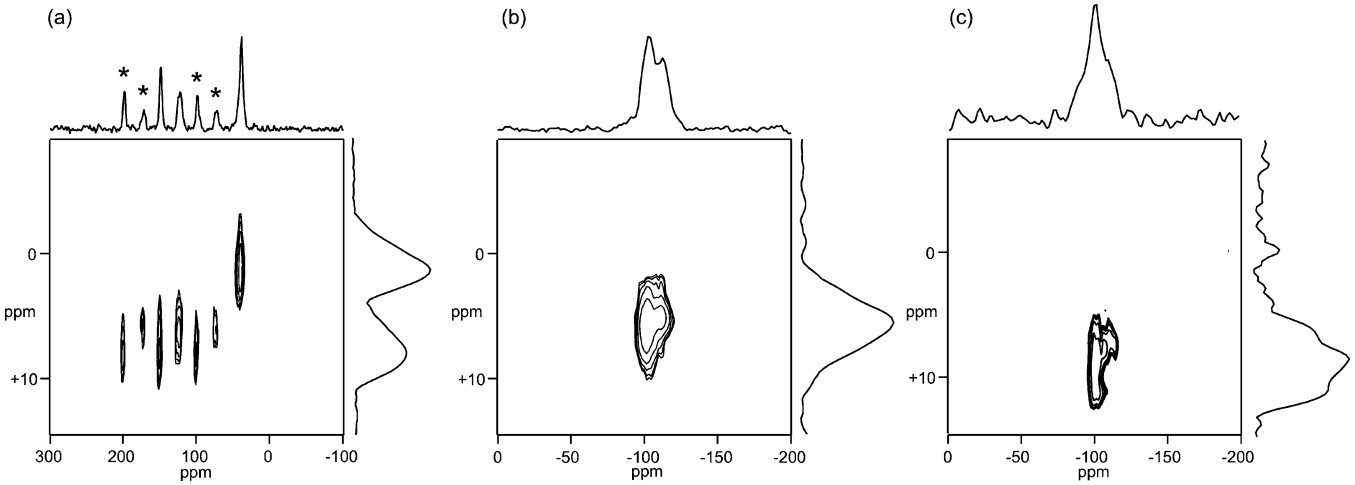

Figure 6. (a) Part of a WIM-24 high-resolution proton−carbon-13 correlation spectrum of the P4VP/silica nanocomposite recorded with the parameters described in the text and carbon-13 (top) and proton (right) skyline projections. Spinning sidebands are marked in the carbon-13 projection with asterisks. (b) Part of a LG-CP high-resolution proton−silicon-29 correlation spectrum of the dried pristine Nyacol silica sol recorded with the parameters described in the text and silicon-29 (top) and proton (right) skyline projections. (c) As for part b but for the P4VP/silica nanocomposite recorded with the parameters described in the text and silicon-29 (top) and proton (right) skyline projections.

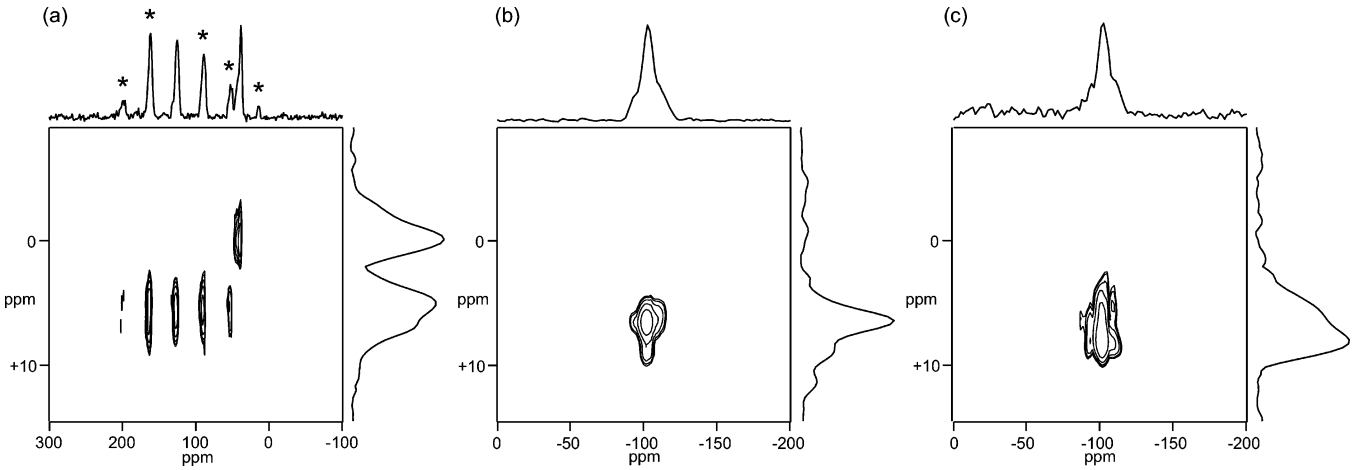

Figure 7. (a) As for Figure 6a but for the PS/silica nanocomposite. (b) As for Figure 6b but for the dried pristine IPA-ST sol. (c) As for Figure 6c but for the PS/silica nanocomposite.

pyridine ring. The remaining proton line has no counterpart in either the proton−carbon-13 correlation spectrum of the nanocomposite or the proton−silicon-29 spectrum of the Nyacol silica sol, and its large δ value indicates some involvement in hydrogen bonding. The most likely explanation is that the interaction of the polymer with the silica surface occurs via a hydrogen bond between the nitrogen atom in a pyridine ring and a silanol hydroxyl proton. This interaction would ensure that the pyridine protons adjacent to the nitrogen were in close proximity with the silicon atoms at the surface.

Figure 7a shows a WIM-24 high-resolution proton−carbon-13 correlation spectrum of the PS/silica nanocomposite. In the carbon-13 skyline projection the isotropic peak at $\delta = 126$ ppm is assigned to the aromatic carbons, with the feature at around $\delta = 40$ ppm being assigned to the aliphatic backbone. As with the P4VP/silica nanocomposite, the aromatic ring and the aliphatic backbone proton resonances are resolved in the high-resolution proton projection. Figure 7b shows a LG-CP high-resolution proton−silicon-29 correlation spectrum of the pristine IPA-ST silica sol. The silicon-29 ω_2 skyline projection shows three peaks, similar to those observed for the Nyacol silica sol. The two-dimensional spectrum shows that the corresponding proton line is somewhat narrower than that observed for the Nyacol silica. Figure 7c shows a LG-CP high-resolution proton−silicon-29 correlation spectrum of the PS/silica nanocomposite. As with the P4VP/silica nanocomposite, a nonspecific van der Waals interaction can be ruled out by the absence of any correlations involving aliphatic protons. On the basis of their δ values, the proton resonances that correlate with the surface silicon site correspond to both surface hydroxyl protons and aromatic ring protons. There is no proton resonance above 10 ppm, suggesting the absence of any hydrogen bonding. Hence, in contrast to the case of P4VP/silica, the most likely model is a π−interaction between the aromatic ring and the silica surface.

Conclusions

In summary, we have demonstrated that solid-state NMR spectroscopy is a powerful tool for probing the nature of the molecular interactions between the organic and inorganic phases of vinyl polymer/silica nanocomposites. In particular, we have shown that the molecular interaction between the polymer and silica phases involves hydrogen bond formation between the pyridine nitrogen and a surface hydroxyl proton for P4VP/silica nanocomposite particles. In contrast, a π-interaction between the aromatic ring and the silica surface is the most likely model for the PS/silica nanocomposite particles. Nonspecific binding interactions do not appear to play an important role in

nanocomposite particle formation in either case. These insights are expected to be useful in the rational design of new types of nanocomposite particles.

Acknowledgment. EPSRC is acknowledged for two postdoctoral research grants for M.J.P. (GR/M22017 and GR/R79814). Dr. P. Greenwood of Eka Chemicals (Bohus, Sweden) and Nissan Chemicals (USA) are thanked for the donation of the Nyacol 2040 and IPA-ST silica sols, respectively. G.K.A. thanks Dr. John Godward (Nottingham) for his assistance during the early stages of this work and the University of Nottingham for financial support.

References and Notes

(1) Chen, C.-W.; Serizawa, T.; Akashi, M. *Chem. Mater.* **1999**, *11*, 1381.
(2) Mitzi, D. B. *Chem. Mater.* **2001**, *13*, 3283.
(3) Vossmeyer, T.; Guse, B.; Besnard, I.; Bauer, R. E.; Mullen, K.; Yasuda, A. *Adv. Mater.* **2002**, *14*, 238.
(4) Manias, E.; Touney, A.; Wu, L.; Strawhecker, K.; Lu, B.; Chung, T. C. *Chem. Mater.* **2001**, *13*, 3516.
(5) Sun, T.; Garces, M. *Adv. Mater.* **2002**, *14*, 128.
(6) Bourgeat-Lami, E. J. *Nanosci. Nanotechnol.* **2002**, *2*, 1.
(7) Barthet, C.; Hickey, A. J.; Cairns, D. B.; Armes, S. P. *Adv. Mater.* **1999**, *11*, 408.
(8) Percy, M. J.; Barthet, C.; Lobb, J. C.; Khan, M. A.; Lascelles, S. F.; Vamvakaki, M.; Armes, S. P. *Langmuir* **2000**, *16*, 6913.
(9) Amalvy, J. I.; Percy, M. J.; Armes, S. P.; Wiese, H. *Langmuir* **2001**, *17*, 4770.
(10) Percy, M. J.; Amalvy, J. I.; Barthet, C.; Armes, S. P.; Greaves, S. J.; Watts, J. F.; Wiese, H. *J. Mater. Chem.* **2002**, *12*, 697.
(11) Percy, M. J.; Armes, S. P. *Langmuir* **2002**, *18*, 4562.
(12) Burum, D. P.; Linder, M.; Ernst, R. R. *J. Magn. Reson.* **1981**, *44*, 173.
(13) Burum, D. P.; Bielecki, A. *J. Magn. Reson.* **1991**, *94*, 645.
(14) van Rossum, B. J.; de Groot, C. P.; Ladizhansky, V.; Vega, S.; de Groot, H. J. M. *J. Am. Chem. Soc.* **2000**, *122*, 3465.
(15) Caravatti, P.; Braunschweiler, L.; Ernst, R. R. *Chem. Phys. Lett.* **1983**, *100*, 205.
(16) Burum, D. P.; Linder, M.; Ernst, R. R. *J. Magn. Reson.* **1981**, *43*, 463.
(17) Sindorf, D. W.; Maciel, G. E. *J. Am. Chem. Soc.* **1983**, *105*, 1487.